Earth's Future

RESEARCH ARTICLE
10.1029/2023EF003823

Performance of Fire Danger Indices and Their Utility in Predicting Future Wildfire Danger Over the Conterminous United States

Guo Yu[1,2,3], **Yan Feng**[1], **Jiali Wang**[1], **and Daniel B. Wright**[3]

[1]Environmental Science Division, Argonne National Laboratory, Lemont, IL, USA, [2]Division of Hydrologic Sciences, Desert Research Institute, Las Vegas, NV, USA, [3]Department of Civil and Environmental Engineering, University of Wisconsin-Madison, Madison, WI, USA

Key Points:

- The correlation between fire danger indices (FDIs) and observed wildfire size are scale dependent
- Sensitivity analysis indicates that the daily minimum relative humidity and wind speed are the most important drivers of fire danger
- Coupling FDIs with regional climate model simulation show higher fire potential in US in future climate

Supporting Information:

Supporting Information may be found in the online version of this article.

Correspondence to:

Y. Feng,
yfeng@anl.gov

Citation:

Yu, G., Feng, Y., Wang, J., & Wright, D. B. (2023). Performance of fire danger indices and their utility in predicting future wildfire danger over the conterminous United States. *Earth's Future*, *11*, e2023EF003823. https://doi.org/10.1029/2023EF003823

Received 18 MAY 2023
Accepted 17 OCT 2023

Author Contributions:

Conceptualization: Guo Yu, Yan Feng, Jiali Wang
Funding acquisition: Yan Feng
Methodology: Guo Yu, Yan Feng, Jiali Wang
Supervision: Yan Feng, Jiali Wang, Daniel B. Wright
Writing – original draft: Guo Yu
Writing – review & editing: Yan Feng, Jiali Wang, Daniel B. Wright

Abstract Predicting current and future wildfire frequency and size is central to wildfire control and management. Multiple fire danger indices (FDIs) that incorporate weather and fuel conditions have been developed and utilized to support wildfire predictions and risk assessment. However, the scale-dependent performance of individual FDIs remains poorly understood, which leads to large uncertainty in the estimated fire sizes under climate change. Here, we calculate four commonly used FDIs over the conterminous United States using high-resolution (4 km) climate and fuel data sets for the 1984–2019 period. The relationships of these four FDIs to the observed wildfire sizes show that higher values of FDIs correlate to larger total fire sizes; this correlation is more robust at larger spatial scales. Sensitivity analysis indicates that the daily minimum relative humidity and precipitation are the most important drivers of the annual mean fire danger. In the instances of extreme fire danger, wind speed becomes a critical factor and should be considered in the calculation of the FDI. To assess the impact of climate change on future fire size, we calculate the present-day and end-of-century FDIs using the 12 km regional climate model simulations. The four FDIs generally predict consistent changes in future fire potential, suggesting an overall higher fire potential in conjunction with a prolonged wildfire season in future climate. Regionally, the four FDIs also reveal similar seasonal patterns as the enhancement arises mostly in spring and summer over the southwest US while in summer and fall over the northern and eastern US.

Plain Language Summary Fire danger index (FDI), a measure used to assess the risk and severity, relies on a combination of weather and fuel conditions. Multiple FDIs have been frequently used to predict and manage the risk of wildfire. However, it is unclear how well these indices work at different scales, causing uncertainty in predicting the likelihood of fire ignition and the potential size of a fire. Here, we analyzed four commonly used FDIs and conducted sensitivity analysis (SA) to determine their most important drivers. SA results indicate that daily minimum relative humidity, precipitation, and wind speed as the most important drivers. In addition, FDIs highly correlate with total fire size at annual and conterminous United States (CONUS) scale and such correlation decreases at finer spatial and temporal scales. We also used a regional climate model simulation to derive FDIs for current and future climate conditions. Our results suggest an overall increase in fire potential and a prolonged wildfire season in the future climate. Moreover, the enhanced fire frequency is projected to occur in spring and summer over the southwest US whereas in summer and fall over the northern and eastern CONUS.

1. Introduction

Wildfire is one of the most devastating natural hazards in the United States, posing a threat to air quality, infrastructure, lives, and property. According to the U.S. National Interagency Fire Center, annual-averaged wildfires in the United States burned 6.8 million acres with a suppression cost of $1.8 billion since 2010 (NIFC, 2020). Wildfire frequency and size is projected to increase in the future due to climate change (e.g., Abatzoglou & Williams, 2016; Brown et al., 2021; Jay et al., 2018), therefore, fire control and management practices will continue to grow in importance. One central objective of wildfire management is to determine wildfire potential (danger) in advance so that forest managers can make informed decisions on how to allocate the available resources. Wildfire potential and danger are interchangeably used in this study, which refers to likelihood that a wildfire will occur and the ability to spread once it has started (e.g., Bradshaw et al., 1984; Burgan et al., 1998;

Hardy & Hardy, 2007). To quantify the wildfire potential, a continuous or categorical scale based on weather conditions and fuel moisture was developed and referred to as fire danger index (FDI). The most commonly used FDIs in North America include the U.S. Geological Survey (USGS) Fire Potential Index (FPI; Burgan et al., 1998), the Canadian Forest Fire Weather Index (FWI) System (Wagner, 1974, 1987), and the Energy Release Component (ERC) and Burning Index (BI) from the National Fire Danger Rating System (NFDRS; Deeming et al., 1977). These fire indices generally consider a set of weather and/or environmental variables such as temperature, relative humidity, wind speeds, and fuel types to determine the potential that a fire may break out, if ignited. In practice, drought monitoring indices such as Keetch-Byram Drought Index (KBDI; Keetch & Byram, 1968) are also often used, as drought conditions are considered to exacerbate the occurrences of wildfires.

Prior to the 1990s, FDIs were generally calculated at the point scale where co-located weather stations and fuel moisture were recorded. The recent advent of remote sensing in weather and earth sciences has made estimates of fire danger over a large domain while at fine-grained level increasingly feasible (see Hardy & Hardy, 2007, for a review of FDIs in the United States). In addition, the massive growth of gridded data from ground-based observations, weather forecasting, and climate modeling also facilitates the estimation of FDIs over a large spatial context with higher temporal resolution (e.g., Baijnath-Rodino et al., 2023). For instance, the USGS Earth Resources Observation and Science Center provides daily forecasts of FPI over the conterminous United States (CONUS) at 1 km resolution using daily weather forecasts from the National Digital Forecast Database (Eidenshink & Howard, 2012). The use of FDIs for fire weather monitoring and risk management has become an important part of the routine operations adopted by various agencies and utility sectors (e.g., Burgan et al., 1998; Di Giuseppe et al., 2016; Hardy & Hardy, 2007).

In addition, FDIs have also been used to investigate the impact of climate change on wildfire size by the mid- and end-of the 21st century (e.g., Abatzoglou & Williams, 2016; Brown et al., 2021), which could be useful for long-term planning and decision making. Although a wealth of FDI products is now available, previous studies that examined the impact of climate change on wildfires were often based on a single FDI (e.g., Tian et al., 2011). Thus, the inherent uncertainty of using an individual index will propagate to the estimated climate change impacts on the wildfire danger. Abatzoglou and Williams (2016) shows different predictability exhibited by multiple FDIs and a drought index in characterizing the total wildfire sizes over the western CONUS. This diversity in predictability implies that use of different empirical FDIs could lead to different estimates of occurrence, intensities, and spatial extents of the fire danger risk. It is thus essential to quantify the performance of FDIs at various conditions and understand the contributing factors that drive the differences in the FDI predictions.

Only a few studies have evaluated the predictability of FDIs with respect to observed fire characteristics, and such evaluations were often performed at regional and seasonal to annual scales (e.g., Abatzoglou & Williams, 2016; Klaver et al., 1997). However, fire monitoring and management practices require reliable metrics and assessment tools at a wide range of spatial and temporal scales from local to the national level and from the near-real time to the annual/seasonal outlook. As climate change would increase fire risks inevitably in the fire-prone regions at present, some historically low-fire-prone regions, such as the northeastern United States, might also become high-risk areas in the future (e.g., Brown et al., 2021). Therefore, there is a critical need to assess the FDI predictability at a range of spatiotemporal scales over the entire CONUS in addition to the western US.

In this study, we first perform a rigorous sensitivity analysis (SA) on four commonly used FDIs (FPI, FWI, ERC, and BI) to unravel the dependence of individual FDI on a set of input weather and environmental variables. The findings will allow us to understand the differences in the FDI predictions. We further analyze the performance of each FDI in predicting the observed fire sizes over the CONUS for the 1984–2019 period at multiple temporal (daily, monthly, and annually) and spatial (grid, regional, and CONUS) scales. Finally, we use the high-resolution regional climate model simulations for the present-day (1995–2004) and projections for late this century (2085–2094) to examine the projected changes in each individual FDI and provide a comprehensive assessment of the seasonal and spatial changes in wildfire potential over the CONUS based on the multiple FDIs.

2. Data Sets

2.1. Wildfire Data

To obtain the long-term wildfire size for quantification of the predictability of FDIs in historical time periods, we use satellite remote sensing data for the 1984–2019 period from the Monitoring Trends in Burn Severity

Project (MTBS; Eidenshink et al., 2007). MTBS provides measurements of fire sizes (i.e., perimeters) larger than 1,000 (500) acres in the western (eastern) CONUS. A total of 13,353 historical wildfires, which do not include prescribed fires, were analyzed in this study. Note that these observed fire sizes represent the perimeter of fire-influenced areas, consisting of inner patches unburned and burned in low, moderate and high severities (Eidenshink et al., 2007).

2.2. Fire Danger Indices (FDIs)

This study considers four commonly used FDIs, calculated at a daily and 1/24° (about 4 km) resolution for 1984–2019: FPI, FWI, ERC, and BI (Figure S1 in Supporting Information S1). These four FDIs are based on both shared (e.g., temperature and precipitation) and unique (e.g., wind speeds in FWI and fuel type in FPI) input variables, representing different aspects of fire conditions. The code for calculating FDIs in this study is adapted from National Center for Atmospheric Research's Fire Indices (NCAR, 2023).

2.2.1. FPI

FPI is an indicator of the wildland vegetation flammability that incorporates both satellite and surface observations (Burgan et al., 1998; Figure S1a in Supporting Information S1). It depends on the NFDRS fuel model map (Bradshaw et al., 1984), normalized difference vegetation index (NDVI; Goward et al., 1991), and an estimate of the so-called 10 hr time lag fuel moisture (Fosberg & Deeming, 1971) which represents the moisture content of small dead fuel (approximate 0.25–1 inch in diameter; Figure S1b in Supporting Information S1). The key assumption of FPI is that fire potential can be assessed if the proportion of live to dead vegetation is accurately defined. The general form of FPI calculation is:

$$\mathrm{FPI} = 100 \times f_{\mathrm{dead}} \times \left(1.0 - \frac{\mathrm{FM}_{10}}{\mathrm{FM}_{\mathrm{extinction}}}\right) \quad (1)$$

where f_{dead} is the proportion of dead vegetation, FM_{10} is the 10 hr fuel moisture and $\mathrm{FM}_{\mathrm{extinction}}$ is the extinction fuel moisture. f_{dead} is calculated using NDVI; $\mathrm{FM}_{\mathrm{extinction}}$ represents the highest level of fuel moisture, making it difficult for a fire to sustain itself.

FPI is shown to highly correlate with the fire occurrences over the U.S. west coast (Klaver et al., 1997), southern Europe (López et al., 2002), and the island of Kalimantan, Indonesia (Sudiana et al., 2003). The USGS Earth Resources Observation and Science Center coupled FPI with a logistic regression model to forecast large wildfires over the CONUS (see Preisler et al., 2009, 2015 for a detailed description).

2.2.2. Fire Weather Index

FWI simulates the effects of air temperature, humidity, vapor pressure deficit, and wind speed on the fuel aridity and consequentially on the fire occurrence and spread (Figure S1b in Supporting Information S1; Wagner, 1974, 1987). First, FWI updates the daily moisture content for three different fuel types (fine fuel, duff, and deep compact organic layers) as nonlinear functions of atmospheric variables (second row in Figure S1b in Supporting Information S1). Next, it calculates the Initial Spread Index, which is a measure of the rate of wildfire spread without the influence of fuel availability. This is done by multiplying two exponential functions: one based on wind speed and the other based on fine fuel moisture. Finally, the Initial Spread Index is scaled by the available fuels (i.e., build up index in Figure S1b in Supporting Information S1) to produce a unitless FWI that represents the intensity of the spreading fire, given the current fuel availability.

Although FWI was designed to describe fire behavior for Canadian forest, such as jack pine stands, the index has proven effective in other regions, such as Australia (Cruz & Plucinski, 2007), New Zealand, and Malaysia (Taylor & Alexander, 2006) as well as globally (Abatzoglou, Williams, et al., 2018).

2.2.3. ERC and BI

Similar to FWI, the NFDRS comprises two primary components (Figure S1c in Supporting Information S1): the ERC, which measures the available fuels, and the BI, which evaluates the potential rate of wildfire spread (Bradshaw et al., 1984; Deeming et al., 1977). First, the NFDRS calculates both live and dead fuel moisture of different fuel types based on various atmospheric variables, such as air temperature, relative humidity, and vapor pressure deficit (Figure S1c in Supporting Information S1). Then, the ERC is calculated as an empirical function

of dead and live fuel moisture, temperature, and relative humidity (Figure S1c in Supporting Information S1). Finally, BI is derived as a nonlinear function of the product of ERC and a fire spread component that depends on both windspeed and fuel availability (Byram, 1959; Figure S1c in Supporting Information S1).

In this study, we applied the latest 2016 NFDRS fuel model (Jolly, 2018) for calculating the ERC and BI. Because the NFDRS accounts for both short-term weather conditions and long-term fuel moisture, ERC, and BI capture both daily fluctuations and seasonal oscillations in wildfire potential. Both ERC and BI have been widely used for describing fire danger, either in operational fire management or research (Di Giuseppe et al., 2016; Finney et al., 2011; Freeborn et al., 2016).

2.3. Meteorological Forcing, Remote Sensing, and Regional Climate Model Simulations

To calculate the four FDIs for the 1984–2019 period, the gridded surface meteorological data (GridMet; Abatzoglou, 2013) at the daily and 1/24° (about 4 km) resolution for the CONUS was used. GridMet aggregates North American Land Data Assimilation System version 2 (NLDAS-2; Mitchell et al., 2004) meteorological forcings and the spatial attributes including orographic effects developed by the Parametrized Regression on Independent Slopes Model (Daly et al., 2008). Gridded daily NDVI at 0.05° (Vermote, 2019) and the NFDRS 1 km fuel model map (Burgan et al., 1997, 1999; Loveland et al., 1991) were also obtained for calculating FPI.

To understand the potential changes of fire danger in the future, we employed two sets of regional climate simulations for the present-day (1995–2004) and the end of the century (2085–2094 under the Representative Concentration Pathways (RCP) 8.5 scenario; Taylor et al., 2012) using the Weather Research and Forecast model (WRF; Skamarock et al., 2008) at a grid spacing of 12 km. These WRF regional model simulations (see Wang & Kotamarthi, 2015) were forced by the boundary conditions generated from the bias-corrected Community Climate System Model version 4 (CCSM4) Global Climate Model (GCM) outputs (Gent et al., 2011). Due to the limited computational resource, Wang and Kotamarthi (2015) only performed six ensembles of 10 years WRF simulation for historic, mid-century, and end of century climate. To demonstrate a relatively robust climate change signal and its impacts on wildfire risks, we focused on end-of-century under RCP 8.5 scenario.

The present-day WRF simulations reproduce the annual and seasonal precipitation and surface temperature climatology reasonably well over the CONUS, while the end-of-century simulations predict a continental-scale warming of ~2–5°C, and over 50% decreases in annual mean precipitation over the southwestern United States (Wang & Kotamarthi, 2015). Our previous study (Brown et al., 2021) examined the similar WRF simulations forced by two other GCM boundary conditions (Donner et al., 2011; Jones et al., 2011) and found consistent changes in KBDI between the present day and end of the 21st century. Therefore, in this study, we consider the FDIs derived from the CCSM4-forced WRF simulations only. The regional climate simulations with WRF do not explicitly account for vegetation dynamics (which are prescribed as static instead) and thus cannot produce the NDVI changes over time. Consequently, we used the satellite retrievals of NDVI from the 1995–2004 period for both present-day and future WRF-based FPI calculations. This caveat might reduce the sensitivity of predicted fire potential in response to the climate change.

3. Methods

3.1. Delta Moment-Independent Sensitivity Analysis (SA)

The delta moment-independent analysis (referred to as Delta; Borgonovo, 2007; Plischke et al., 2013) is a global SA technique that assesses the influence of inputs on an entire distribution, rather than certain orders of statistical moments of model output. Unlike some other SA methods (e.g., the variance-based Sobol method; Sobol, 2001), the Delta method we used here does not require independence among inputs. These features make the Delta method well-suited for performing SA for the FDIs, since most input variables are correlated with each other to a certain degree (e.g., precipitation and relative humidity) and may influence the output distribution without disturbing a particular moment. A more detailed description of the Delta method can be found in the Supporting Information S1 and Borgonovo (2007). We provide a summary in the following paragraphs:

Considering that all the model inputs $\overline{X}$ are free to vary, the output Y has the unconditional probability density function (PDF) $f_Y(y)$. Then, when one of the inputs X_i is fixed, a conditional PDF $f_{Y|X_i}(y)$ is generated. The separation between them is defined as

$$s(X_i) = \int |f_Y(y) - f_{Y|X_i}(y)| \mathrm{d}y \tag{2}$$

Since the separation $s(X_i)$ is dependent on the random input X_i, the expected separation is given by E_{X_i}, ranging from 0 to 2. Finally, the Delta measure, δ_i, is defined as half of E_{X_i}.

$$\delta_i = \frac{1}{2} E_{X_i}[s(X_i)] = \frac{1}{2} \int f_{X_i}(x_i) \left[\int |f_Y(y) - f_{Y|X_i}(y)| \mathrm{d}y \right] \mathrm{d}x_i \tag{3}$$

The possible values of δ_i range between 0 and 1, and δ_i is zero when Y is independent of X_i and unity when Y is a univariate function of X_i. In this study, Delta SA was performed for each FDI using an open source Python library, SALib (Herman & Usher, 2017). Figure S2 in Supporting Information S1 illustrates how FPI distributions vary with changes in each input variable, along with their calculated Delta sensitivities.

To calculate the Delta SA for each FDI, we performed random sampling of 50,000 pairs of computed FDIs and their corresponding inputs across the CONUS using data from 1984 to 2019 (see Section 2.2) (A prior test using an increasing number of sample size N found that the Delta measures stabilize around N = 10,000; thus, N = 50,000 ensures a large sample size as well as computational efficiency). This sampling process was repeated to generate 100 realizations of the Delta measures to represent sampling uncertainty.

3.2. Trend and Correlation

Trend analyses were conducted on the annual occurrences of MTBS wildfires during the period of 1984–2019 at both regional (Level-2 Eco-regions; CEC, 1999) and CONUS scales. The Level-2 eco-region classification system divides the US into 50 distinct eco-regions based on factors such as climate, geology, topography, vegetation, and soils. We applied nonparametric Mann–Kendall (MK) tests (Mann, 1945), which does not require the data to conform any specific statistical distribution, for detecting monotonic trends in time. To understand the relationships between fire size and four FDIs, we calculated the Spearman's rank correlation (Spearman, 1904) at nine different spatiotemporal scales, ranging spatially from single grid, to regional and CONUS scales; and temporally from daily, to monthly and annually. For each scale, the logarithm of corresponding total wildfire size from MTBS is correlated with the four FDIs estimated from a combination of assimilated meteorological forcings (NLDAS-2), satellite vegetation (NDVI), and fuel maps (NFDRS).

4. Results

4.1. The Seasonality and Long-Term Trends of Historical Wildfires

We analyzed a total of 13,353 observed MTBS wildfire occurrences over the CONUS from 1984 to 2019. Seasonal variations of annual wildfire frequency summing over the CONUS reveal two dominant peaks, a primary one in August and a secondary peak in April, followed by an additional local maximum in November (Figure 1a). To determine the spatial distribution of wildfire seasonality, we applied a 2D Gaussian filter with a size of 132 km and a standard deviation of 16 km to compute wildfire occurrence (i.e., day of year) over each NLDAS-2 4 km grid cell which have been further grouped into four seasons: spring (March–May), summer (June–August), fall (September–November), and winter (December–February; Figure 1b). Most wildfires in the western US occurred in summer when strong convective storms are frequent and associated with intense lightning for the onset of fires (Balch et al., 2017). This is consistent with the peak season of the total fire counts over the CONUS, suggesting that the wildfires in the western US dominate the total number of wildfires in the country. A few exceptions include northwest Oregon, central Wyoming and North Dakota, and Central and Southern California, where wildfire seasons dominate in fall (Figure 1), for example, the latter is coincident with the hot and dry conditions driven by the Santa Ana winds (ongoing work). In the eastern US, wildfires mostly occurred in the spring, except the central Appalachians where wildfires occurred more frequently in fall. The spring wildfires in eastern US are suggested to be associated with a dry-down after snowmelt and ahead of summer rainfalls (e.g., Gleason et al., 2019; Westerling, 2016).

MK trend tests (two sided) show that the number of wildfires and their total burned areas over the CONUS have increased significantly in the last 36 years by 94% and 337%, respectively (Figure 1c), consistent with other recent studies (e.g., Boisramé et al., 2022; Iglesias et al., 2022). The percent increase in total wildfire size is more

10.1029/2023EF003823

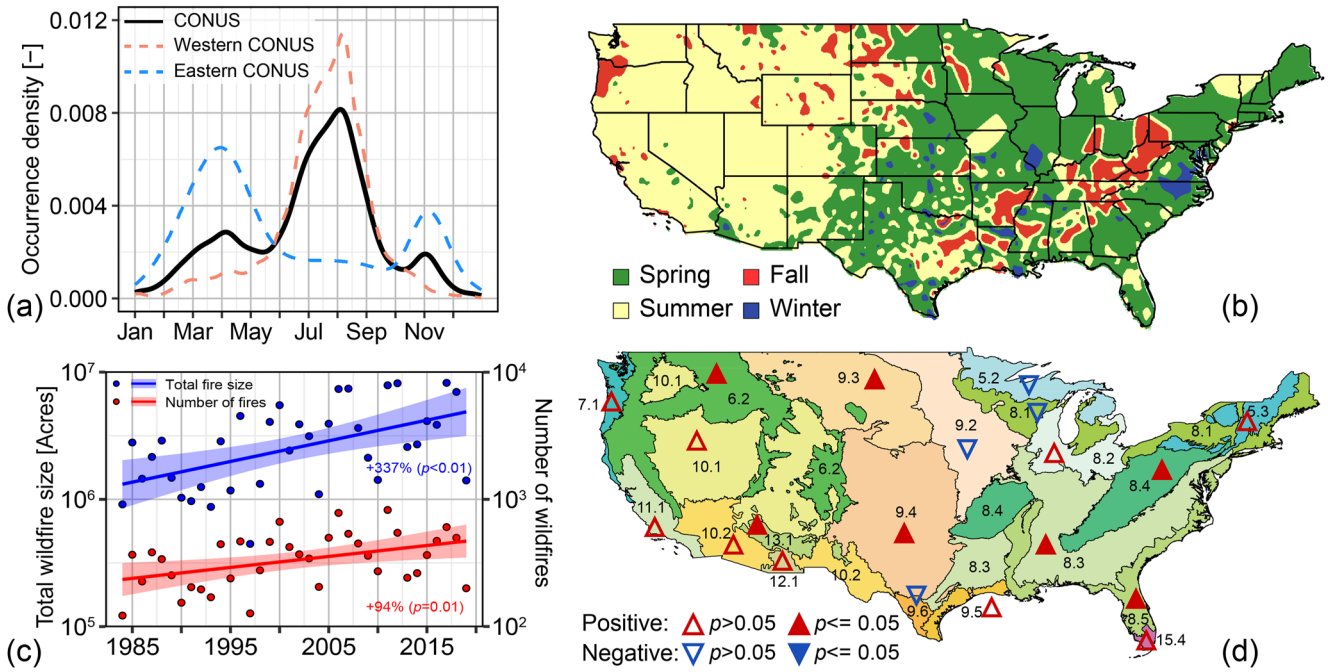

Figure 1. The seasonality of historical wildfires (a) and its spatial distribution (b) over the CONUS. Trends in annual total wildfire size and frequency over the CONUS (c) and each individual eco-region (d). Fire seasons in panel (b) are grouped into spring (March–May), summer (June–August), fall (September–November), and winter (December–February). Filled (unfilled) triangles in panel (d) indicate significant (insignificant) trends at 5% level. Trends in number of wildfires over eco regions are not shown in panel (d) though they are comparable to trends in the fire size. The name of each eco-region in panel (d) can be found in Table 1.

than three times larger than the increase in wildfire frequency (Figure 1c), indicating the mean fire size has also increased in the last four decades. The increase in wildfire size is prevalent across different eco-regions over the CONUS except for the four regions which show insignificant decreases (Figure 1d). They are mostly over the northwestern US, including the Mixed Wood Shield (eco-region 5.2) and Plains (eco-region 8.1), and Temperate Prairies (eco-region 9.2).

In general, the more frequent and enlarged wildfires are attributed to both increasing drought severity (Dennison et al., 2014; Gamelin et al., 2022) and fire suppression activity that leads to fuel build-up (Brotons et al., 2013). In addition, the interannual variabilities in wildfires size and frequency are suggested to link to the interannual variability in precipitation, surface air temperature, and vapor pressure deficit (Figure 1c; Abatzoglou, Williams, et al., 2018). For example, we found that the mean annual temperature over the CONUS during the 1984–2019 period correlates (at 5% significance level) with the corresponding wildfire sizes and frequencies, with the Spearman coefficients of 0.54 and 0.59, respectively. This strong link between fire and weather on the annual basis suggests that the antecedent meteorological conditions (e.g., precipitation and temperature) could be used in predicting interannual variations and long-term trend of wildfire sizes (Abolafia-Rosenzweig et al., 2022).

4.2. SA of FDIs

To better understand the differences in the predicted fire potential by various FDI, we first quantify the dependence of FDIs on a set of the atmospheric and surface conditions, which are used in any of the four FDI formulations. Delta measures (Equation 2) in statistics are calculated for each individual FDI and their values that exceed 95th percentile over the CONUS for the 1984–2019 period, as shown in Figure 2. Among all the input variables considered, daily minimum relative humidity (RH_{min}) is identified as the most or second most dominant parameter in calculating the four different FDIs (Figure 2a), as well as for the upper tail only of each FDI (>95th percentiles; Figure 2b). The latter denotes the large fire potential indicated by FDIs. This strong dependence on RH_{min} by the four FDIs is consistent with the fact that all of them use RH_{min} as an input to estimate the dead fuel moisture, which plays an important role in determining the fire behavior. In contrast, some of the other shared input variables, like T_{max}, show different Delta measures for the four FDIs, indicating that each FDI was designed specifically to characterize the fire danger from varied aspects. Thus, the same weather variable may

10.1029/2023EF003823

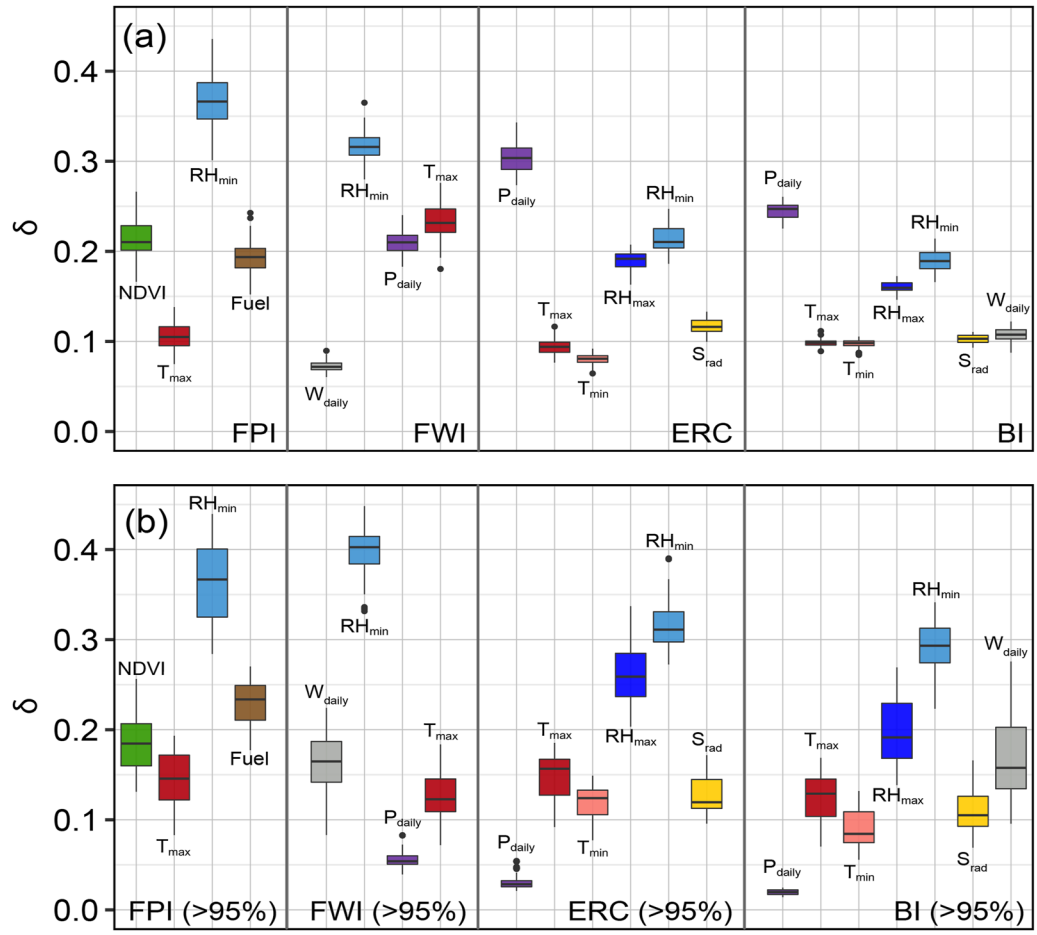

Figure 2. Delta-based global sensitivity analyses for (a) four fire danger indices (FDIs) and (b) FDIs that exceed the 95th percentile. Variables: daily precipitation (P_{daily}), daily maximum and minimum temperature (T_{max} and T_{min}), daily maximum and minimum relative humidity (RH_{max} and RH_{min}), fuel type (Fuel), weekly maximum NDVI (NDVI), and daily mean shortwave radiation (S_{rad}) and wind speed (W_{daily}).

carry different weights in assessment of the wildfire danger, depending on the choice of the FDI. As a result, some FDIs such as FWI would give prominence to the hot (high T_{max}) and dry (low RH_{min}) conditions for driving high fire risks, while the more complicated FDIs such as ERC and BI place relatively less weight on surface air temperature, as they also take the fuel moisture (or flammability) on the ground into account, which is related to daily precipitation (low P_{daily}).

For extreme FDI values—those exceeding the 95th percentile—the SA shows largely consistent results with the entire distribution of the FDI values (Figure 2a), except that the role of wind speed (W_{daily}) has been highlighted (Figure 2b). Among the four FDIs, only FWI and BI account for the spread of wildfires and depend on wind speed. Notably, W_{daily} has the least influence on both FWI and BI when considering all the predictions (Figure 2a) but plays a remarkably larger role on the predicted values that exceed 95th percentiles (Figure 2b). This reflects that surface wind speed may be less important under the low or moderate fire potential compared to other environmental conditions, but become more critical under the high-fire potential (e.g., high temperature and low humidity), as strong winds can intensify the spread of wildfires and exacerbate the fire severity after fires break out. Mathematically, it is consistent with the formulation of wind speeds in calculating FWI and BI, in which the exponential impacts of wind speed are "triggered" when other factors are also indicative of high fire potentials (see Figure S3 in Supporting Information S1 for an example showing FWI as a function of wind speed).

The most sensitive input parameter for each FDI at the grid level varies both spatially and across different FDIs (Figure S4 in Supporting Information S1). In the western CONUS, RH_{min} and P_{daily} are the two most sensitive input variables, while in the eastern CONUS, NDVI, T_{max}, and P_{daily} are the most sensitive variables for FPI, FWI,

10.1029/2023EF003823

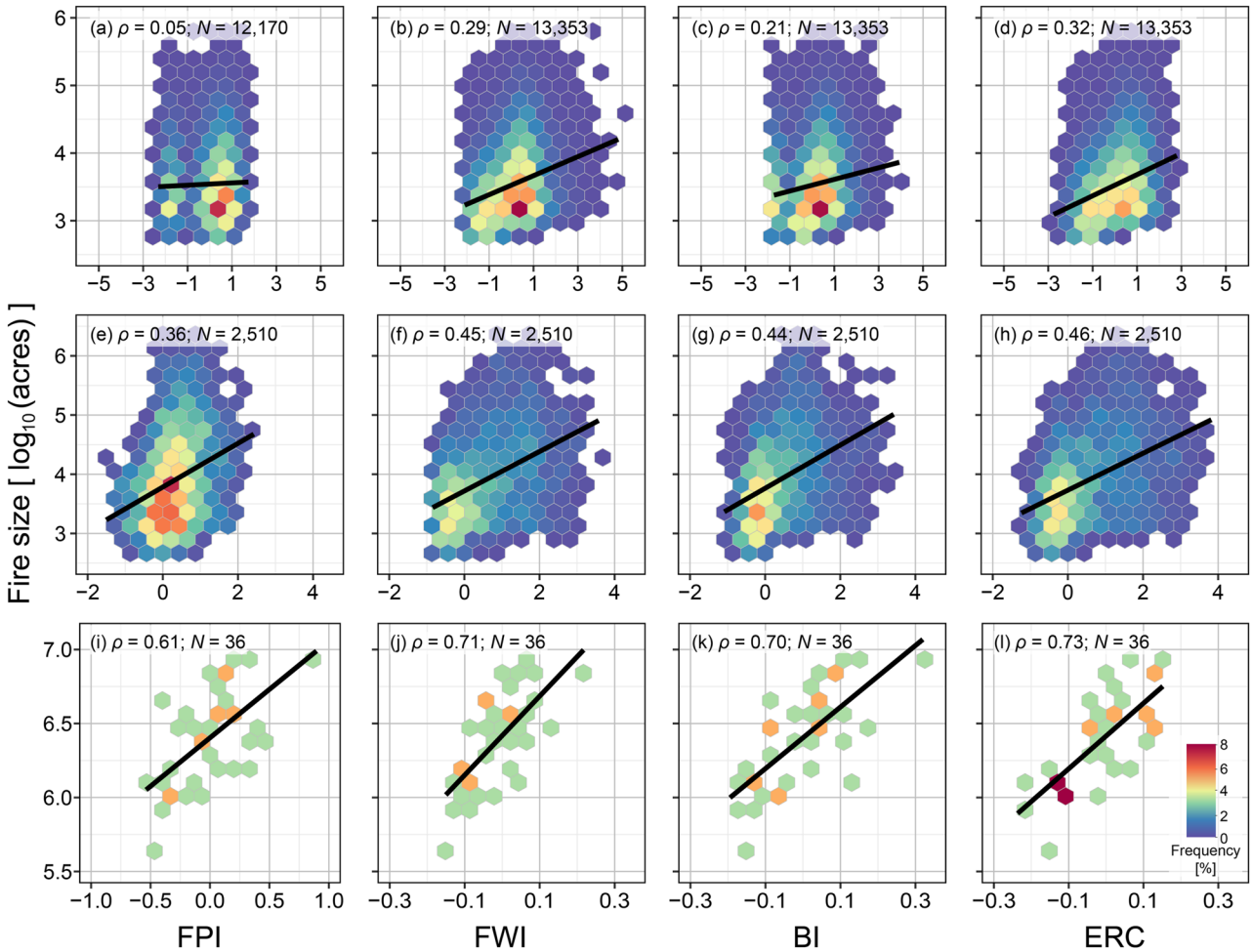

Figure 3. Relationships between total wildfire sizes (on the logarithmic scale) and mean normalized fire danger indices for three different scales: grid and daily (a–d), regional and monthly (e–h), and CONUS and annually (i–l). Spearman's correlation (ρ) and sample size (N) are given in the top of each panel. Correlations in all panels are statistically significant.

and ERC and BI, respectively. Clearly, the estimated fire potential by a specific FDI relies on what input parameters it considers, and the relative importance of each input parameter based on the formulation. The results of SA also highlight that even these simple FDIs represent complex, nonlinear systems, and the expectations inherent in its formulation can be different from model performance. As those input parameters have different variability in time and space, it would lead to the diverse predictions of wildfire potential by the FDIs on different scales. Next, we will examine the scale dependence of FDIs in predicting the wildfire size in observations.

4.3. Correlation Between Fire Size and FDIs

We calculated the Spearman correlations between the mean FDIs and the total wildfire sizes at three different spatiotemporal scales: grid and daily (Figures 3a–3d), regional and monthly (Figures 3e–3h), and CONUS and annually (Figures 3i–3l). For example, regional and monthly values (Figures 3e–3h) refer to as correlation between the mean FDIs and the total wildfire sizes in each eco-region for every month. In general, all correlation coefficients are statistically significant and increasing with coarsening of the spatiotemporal scales, independent of the FDI option. All indices show low but significant correlations with fire sizes at the grid and daily scale, while they show more robust predictability for regional and monthly and CONUS and annually fire size (Figures 3i–3l). Specifically, the weak correlations depicted in the panels (a) to (d) show that the daily predictions of FDIs at the ~4 km grid spacing overestimate the variability in the wildfire sizes. It means that while the daily and local changes of those input parameters (weather and surface fuel conditions) for FDI may

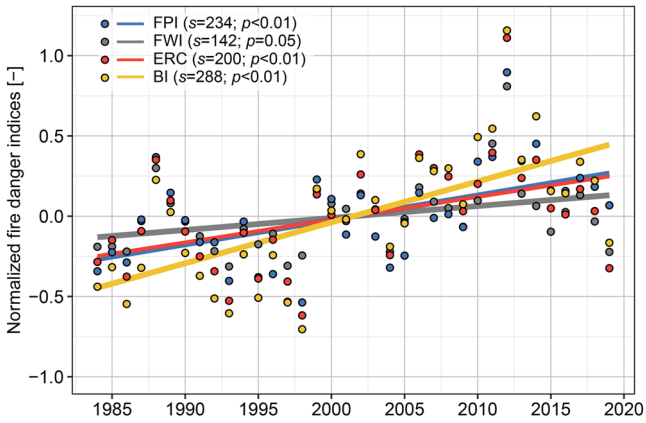

Figure 4. The normalized annual mean FPI, Fire Weather Index, Energy Release Component, and Burning Index over the CONUS and their fitted simple linear regressions. The Mann–Kendall slope and the corresponding *p*-value for each Fire danger index is shown.

frequently point to the favorable conditions for wildfires, in reality, the occurrences of wildfires are much less in counts or less severe in burned areas, indicated by the weak responses ($\rho < 0.32$) of the observed fire sizes to the FDI variations. This finding reinforces the challenges existing in the local-scale, near real-time wildfire predictions, as the occurrences and sizes of wildfire at these fine scales are highly variable and influenced by many local factors including ignition causes (human-vs. lightning-related; e.g., Abatzoglou, Balch, et al., 2018; Balch et al., 2017), fire suppression activities (e.g., Steel et al., 2015), and housing and road densities (e.g., Sturtevant & Cleland, 2007). These factors along with other unknown processes subdue the influences of the input parameters accounted by the existing FDIs. On the other hand, the dominance of those input parameters in predicting the wildfire potential is revealed gradually with the increased correlation against the larger-scale wildfire observations, making the FDI predictions more reliable over a large context.

Besides their strong correlations with fire size, four FDIs at the CONUS-wide annual scale also show similar upward trends in time and strong interannual variability for the 1984–2019 period (Figure 4), consistent with the historical wildfire data over the CONUS in Figure 1c. Four annual mean FDIs indicate the monotonic positive trends with the MK tests (Figure 4). We also applied the MK tests to the annual mean and 95th percentiles of four FDIs for each eco-region to assess their trends (Table 1). Similar to the CONUS scale, trends in all the four FDIs on the regional scale also reproduce the long-term increases in the observed fire size across most of the eco-regions (Figure 1d), except for eco-regions located in northwestern US, like Mixed Wood Shield (eco-region: 5.2) and Plains (eco-region: 5.3). This suggests that either of the four FDIs

Table 1
Mann–Kendall Trend Test (Two Sided) for the Annual Mean and 95th Percentile of Four Fire Danger Indices for Each Eco-Region

Eco-region	FWI (mean)	FWI (95%)	FPI (mean)	FPI (95%)	ERC (mean)	ERC (95%)	BI (mean)	BI (95%)
5.2—Mixed Wood Shield	↑	↑	↑*	↑	↓	↓*	↑	↓
5.3—Atlantic Highlands	↑	↑	↑*	↑*	↓	↓	↑*	↑
6.2—Western Cordillera	↑	↑	↑	↑	↑*	↑*	↑*	↑*
7.1—Marine West Coast Forest	↑	↑	↓	↑	↑	↑	↑	↑
8.1—Mixed Wood Plains	↑	↑	↑*	↑*	↓	↓	↑*	↑
8.2—Central Plains	↑	↑	↑*	↑*	↑	↑	↑*	↑*
8.3—Southeastern Plains	↑	↑	↑*	↑*	↑*	↑	↑*	↑*
8.4—Appalachian Forest	↑	↑	↑*	↑*	↑*	↑	↑*	↑*
8.5—Southeast Coastal Plains	↑	↑	↑*	↓	↑*	↑	↑*	↑*
9.2—Temperate Prairies	↑	↓	↑*	↑*	↑	↓	↑*	↑
9.3—West-central Semiarid	↓	↓	↓	↑	↓	↓	↑*	↑
9.4—South-central Semiarid	↑*	↑*	↑*	↑*	↑*	↑	↑	↑*
9.5—Texas-Louisiana Coastal Plain	↑	↑	↑	↑	↑*	↑	↑*	↑*
9.6—Texas Semiarid Plain	↑	↑	↑	↑	↑	↑	↑*	↑*
10.1—Cold Deserts	↑	↑	↑	↑*	↑*	↑*	↑*	↑*
10.2—Warm Deserts	↑*	↑*	↑*	↑*	↑*	↑*	↑*	↑*
11.1—Mediterranean California	↑	↑*	↑	↑*	↑*	↑*	↑*	↑*
12.1—Western Sierra	↑*	↑*	↑*	↑*	↑*	↑*	↑*	↑*
13.1—Upper Gila Mountains	↑*	↑*	↑*	↑*	↑*	↑*	↑*	↑*
15.4—Everglades	↑	↑	↑*	↓	↑*	↑	↑*	↑*

Note. Arrows with asterisk are significant at the 5% level.

10.1029/2023EF003823

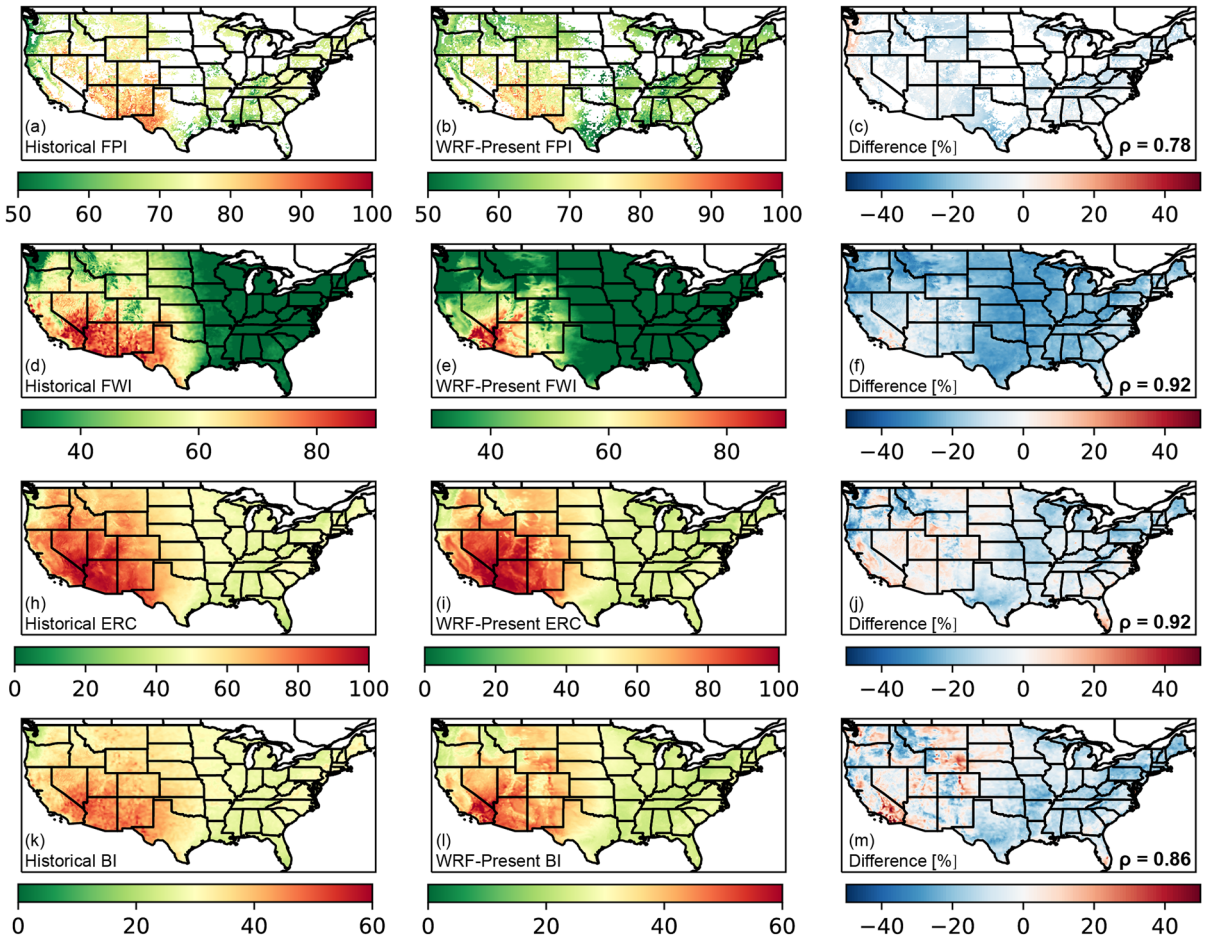

Figure 5. The derived 95th percentiles of FPI, Fire Weather Index, Energy Release Component and Burning Index using 1984–2019 observed forcings (a, d, h, and k) and WRF simulated present-day forcings (b, e, i, and l), respectively. Their percent differences and Spearman's correlation are shown in panels (c), (f), (j), and (m).

is a reliable indicator of annual wildfire changes in terms of fire size (i.e., burned area), and could be used for long-term and annual fire forecasts over each eco-region. Down to the seasonal or intra-annual variability, daily predictions of the four FDIs at the regional scale also reproduces the observed fire seasonality, as the season of high FDIs approximately coincides with the occurrence of historical wildfire across different eco-regions (Figure S5 in Supporting Information S1).

4.4. Future Changes in WRF-Based FDIs

The assessment of the FDI predictability against the wildfire observations in the historical time periods suggests that FDIs could be used to investigate the long-term changes of wildfire potential due to climate change, amid some regional differences. To encompass the uncertainty due to the choice of FDI, we derived WRF-based, four FDIs for both the present day (1995–2004) and future periods (2085–2094) at daily and grid (12 km) scales. High FDI values are indicative of critical wildfire weather conditions and are associated with large wildfire size across different scales (Figure 3). Consequently, we focus on the climate change impacts on the extreme wildfire conditions in this subsection, which are represented by changes in the number of days per year that exceed the 95th percentiles of the daily predictions of each individual FDI.

The present-day WRF-based FDIs are first evaluated with the predictions based on the observational GridMet forcing. Figure 5 shows that the derived 95th percentiles for the four WRF-based FDIs are overall comparable and significantly correlate with the corresponding values derived from the observational forcing. In general, 95th percentiles of different FDIs show consistent spatial pattern, which is highest for the Southwest, followed by the Northwest, Midwest and eastern US (Figure 5). The differences in these two sets (Figure 5) of FDIs are

10.1029/2023EF003823

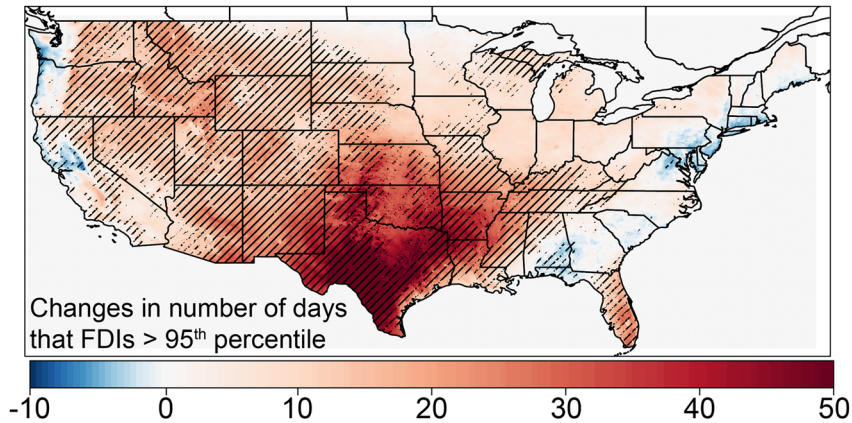

Figure 6. WRF-based changes in the mean number of days that exceed the 95th percentile of four fire danger indices (FDIs) from the present day to the late 21st century. Dashed lines denote the directions of changes (i.e., positive or negative) are consistent among four FDIs. Changes in the number of days that exceed the 95th percentile for each individual FDI are shown in Figure S5 in Supporting Information S1.

mainly due to the biases in the WRF simulations of the meteorological forcing such as temperature, relative humidity, surface winds and incoming solar radiation. As shown in Figure 2b and discussed in Section 4.2, the 95th percentile of FDIs is nearly insensitive to the calculated daily precipitation. Among the four FDIs, it is not surprising that the WRF-based FPIs have the smallest uncertainty introduced by the input parameters (e.g., small negative differences in Figure 5c), as it only depends on RH_{min} and T_{max}. Inclusion of the surface winds at noon (W_{noon}) in the FWI calculation enhances the negative bias in the WRF-based predictions over most of the domain except for some portions of the southwestern US, suggesting that WRF might underestimate W_{noon} compared to the observations (Figure 5f).

Compared to FPI or FWI, more complex ERC and BI, which account for more input weather variables, show negative and positive biases on the eastern and western US, respectively (Figures 5h–5m). The biases in the WRF-predicted daily mean surface windspeed (W_{daily}) further enhances the negative or positive biases with ERC and BI (with W_{daily}). This shows that although the predictability of FDI may be generally improved with more input parameters considered (Figure 3), it also requires the increased fidelity of those weather and climate model simulations, for example, surface wind fields. Out of the four FDIs, ERC is the best represented by WRF with the largest correlation and smallest percent differences, despite the uncertainties propagated from the WRF-simulated meteorological forcings.

Assuming that the intrinsic biases in the WRF-based FDI predictions would be similar for the present day and future projection, the uncertainty in the FDI differences would be small, that is, less than those in Figure 5. This allows us to use the WRF calculations of FDIs to quantify the impact of climate change. We calculated the changes in the number of days that exceed the 95th percentiles of four FDIs between using WRF-present and -future simulated forcings (Figure S6 in Supporting Information S1). The changes in the number of days averaged from the four FDIs is shown in Figure 6. The mean occurrence frequency of FDIs > 95th percentile is projected to increase by, at least, 10 days per year across the CONUS, implying a longer season of extreme wildfire conditions (Figure 6). Particularly, the potential extreme wildfire days (i.e., FDIs > 95th percentile) in Southern Great Plains, including Kansas, Oklahoma, Arkansas, and Texas, are projected to increase by more than 40 days, indicating these places are more vulnerable to the future wildfire risks.

On the contrary, there are few spots along the western and eastern coasts showing slight decreases in number of days that FDIs > 95th percentile (Figure 6). They are mainly in Marine West Coast Forest (eco-region: 7.1) and Southeast Coastal Plains (eco-region: 8.5). These decreases in wildfire potentials are attributable to the projected increase in future precipitation and relative humidity along these coastal regions. This is also in line with the projected increases in annual precipitation by other RCMs (e.g., Almazroui et al., 2021; Easterling et al., 2017; Gutzler & Robbins, 2011; Lynch et al., 2016). Another reason is that four FDIs, especially for their extreme values, are highly sensitive to the relative humidity, a slight change in which can result in very different wildfire hazards (Figure 2 and Section 4.2).

Table 2
Percent Differences in Mean (μ), Standard Deviation (σ), and 95th Percentile of Four Fire Danger Indices for Each Eco-Region Using Between WRF Present-Day and Future Simulations

	FWI [percent difference]			FPI [percent difference]			ERC [percent difference]			BI [percent difference]		
Eco-region	μ	σ	95th	μ	σ	95th	μ	σ	95th	μ	σ	95th
5.2—Mixed Wood Shield	42	52	26	6	3	1	8	4	2	4	4	3
5.3—Atlantic Highlands	34	23	21	4	−1	−2	5	2	0	1	−2	−4
6.2—Western Cordillera	32	16	16	10	7	5	14	5	6	9	5	5
7.1—Marine West Coast Forest	13	6	11	−1	−2	−2	−2	−1	−2	−4	−3	−4
8.1—Mixed Wood Plains	34	39	24	6	1	0	7	3	2	4	2	1
8.2—Central Plains	36	33	31	7	3	1	8	2	5	6	2	2
8.3—Southeastern Plains	32	27	26	4	2	1	9	3	4	8	5	5
8.4—Appalachian Forest	41	35	32	6	2	1	10	6	7	7	5	6
8.5—Southeast Coastal Plains	24	18	21	1	1	1	8	5	4	6	4	4
9.2—Temperate Prairies	42	34	33	12	8	6	11	3	6	9	5	6
9.3—West-central Semiarid	33	16	21	10	8	6	9	2	6	6	5	5
9.4—South-central Semiarid	59	36	41	13	8	7	20	4	11	19	10	13
9.5—Texas-Louisiana Coastal Plain	59	46	58	9	8	6	15	5	10	17	8	10
9.6—Texas Semiarid Plain	75	49	52	19	14	13	26	7	16	32	13	24
10.1—Cold Deserts	22	10	12	10	3	3	11	−2	3	9	4	6
10.2—Warm Deserts	23	4	11	8	1	4	10	−7	2	11	0	5
11.1—Mediterranean California	15	4	5	5	1	2	4	−1	0	5	0	2
12.1—Western Sierra	31	11	17	9	2	5	14	−2	5	14	4	8
13.1—Upper Gila Mountains	35	15	18	11	2	4	16	−4	6	15	5	9
15.4—Everglades	26	22	23	6	3	3	12	7	10	10	4	1

We also investigated the changes in four FDIs over each eco-region. Future FDIs in all eco-regions are, more or less, projected to increase in mean (μ), variability (σ), and the 95th percentiles, implying that wildfire hazard in future will be a more challenging issue to the nation (Table 2; Figure S7 in Supporting Information S1). Larger variability and higher upper tail values in future FDIs suggest that the values are more spread out to high values. In terms of the changes in the μ and σ, four FDIs show consistent results that the semiarid, central south (eco-regions: 9.3, 9.4, 9.5, and 9.6) indicate the largest increases. This is roughly consistent with the regional drought trends over the last four decades (Ficklin et al., 2015). Conversely, both FPI, ERC, and BI, show a slight decrease (<5%) in future mean values over the Marine West Coast Forest (eco-region: 7.1), attributable to the projected wetter climate in future.

In addition, projected future increases in four FDIs also reflect considerable seasonal variation across the eco-regions (Figures S8–S11 in Supporting Information S1). In southwestern US (eco-regions: 10.1, 10.2, 12.1, and 13.1), the largest increases in four FDIs occur in spring and summer, while in northeastern US (eco-regions: 5.2, 5.3, and 8.3) they occur in fall. Similarly, we derived the mean number of days among four FDIs that exceed 95th percentiles over 20 eco-regions and four seasons (Figure 7). In the southwestern US, the extreme wildfire season has been prolonged by more than 20 days and most increases occur in the spring and summer. In the northern and eastern US, the extreme wildfire season increased by around 10 days, and they mostly occur in summer and fall. What is more, a longer fire season in the winter is also evident for some eco-regions, especially in the Texas-Louisiana Coastal Plain (eco-region: 9.6).

5. Summary and Conclusions

FDIs have emerged as important decision-making tools in fire control and risk management. However, understanding of their underlying processes and predictive power remains limited. This poses significant challenges

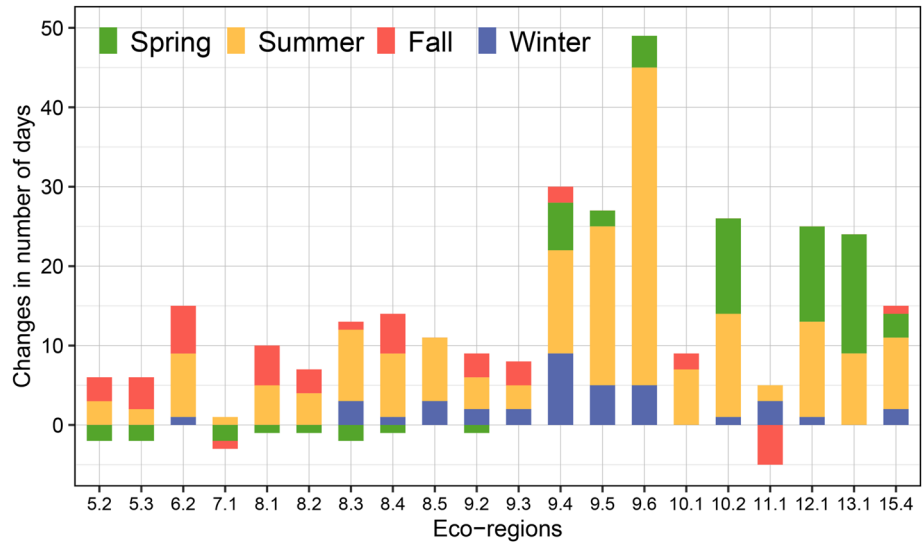

Figure 7. The averaged changes in the number of days exceeding the 95th percentiles over 20 eco-regions and four seasons.

in the application of FDIs. In this study, we applied the Delta SA method to four FDIs and found that the most dominant parameter is minimum relative humidity for FPI and FWI while daily precipitation for ERC and BI (Figure 2a). In addition, extreme values of FWI and BI responds strongly to windspeed, reflecting the determinant role of winds in blowing flame and spreading fire under severe fire conditions. These findings facilitate the interpretation of predictions from different indices and provide insights into future improvements. For example, wind speed should be taken into account for those FDIs that currently do not include it, especially for severe, large fires.

This study investigated the correlation between four FDIs and fire size at three different spatial and temporal scales during the 1984–2019 period. The performance among four FDIs are comparable while BI slightly outperforms other three FDIs at all scales. In addition, four individual FDIs show better performance in predicting the fire size at coarse (e.g., regional and monthly) than at fine (e.g., grid and daily) resolutions. Despite the low correlation between the FDIs and fire size at the fine scale, the interannual variability and long-term trends in the four FDIs are consistent with patterns in the number of observed historical fire events (Figure 4). Furthermore, one must be cognizant of two important factors when interpreting FDIs: (a) fire danger aims to assess the potential of fire occurrence and size at a broad scale in space and time rather than to forecast individual fire behavior; and (b) in practice, FDIs are used in conjunction with more detailed fire behavior analysis (e.g., Finney, 2006).

We further derived four FDIs for current (1995–2004) and future (2085–2094) climate conditions using high-resolution dynamically downscaled regional climate simulations. We must acknowledge that the results we presented may contain uncertainties, considering that the WRF projections utilized in this study were based on a single GCM and under the RCP 8.5 scenario. However, the model does not project a significant change in relative humidity (our preliminary results) and wind speeds (Wu et al., 2022), and the fuels and NDVIs are static in time, thus the changes in FDIs are primarily driven by the changes in air temperature given its relatively high sensitivity. Thus, we do not expect the conclusion of this study to be changed even when we use WRF driven by other GCMs as used by Brown et al. (2021). Despite these limitations, WRF-based results resemble the spatial patterns of observation derived FDIs with a high Spearman's correlation coefficient, demonstrating the adequacy of WRF simulation in estimating the FDIs.

To further limit the impact of model biases on estimated FDIs, we focus on the projected changes in FDI values and in the number of days when FDIs exceed the 95th percentiles. Results show that the mean and variability of four FDIs are projected to increase across all eco-regions except for few places along the coastal region due to projected wetter climate in future. Projected increases mainly occur in the spring and summer over southwestern US while summer and fall over the northern and eastern US. The future extreme wildfire season is projected to become longer, especially in south-central CONUS which show increases in FDIs > 95th percentile by more than 30 days per year. Many of these projected regions, particularly New Mexico, Texas, and Louisiana, encompass

counties with high social vulnerability (Flanagan et al., 2018); this implies that there is a potential for wildfire to exacerbate poverty and elevated safety risks due to crowded housing and limited transportation access.

Data Availability Statement

GridMet forcings are available at https://www.climatologylab.org/gridmet.html (Abatzoglou, 2013); NDVI data is from NOAA Climate Data Record and available at https://www.ncei.noaa.gov/metadata/geoportal/rest/metadata/item/gov.noaa.ncdc:C01558/html (Vermote, 2019); Monitoring Trends in Burn Severity Project data can be downloaded directly from the project website (Eidenshink et al., 2007).

Acknowledgments
This work is supported by the Laboratory Directed Research and Development program of Argonne National Laboratory provided by the U.S. Department of Energy (DOE) Office of Science under Contract No. DE-AC02-06CH11357. We acknowledge Dr. Robert Burgan, Dr. Haiganoush Preisler and Emily Brown for their support in calculating fire indices. We acknowledge Dr. Tim Brown from Desert Research Institute for an internal review. YF acknowledges the support of the DOE Office of Science, Office of Biological and Environmental Research, Atmospheric System Research (ASR) program and Earth System Model Development (ESMD) program. All the analysis was performed by using the computing cluster (Bebop) operated by the Argonne's Laboratory Computing Resource Center.

References

Abatzoglou, J. T. (2013). Development of gridded surface meteorological data for ecological applications and modelling [Dataset]. International Journal of Climatology, *33*(1), 121–131. https://doi.org/10.1002/joc.3413

Abatzoglou, J. T., Balch, J. K., Bradley, B. A., & Kolden, C. A. (2018). Human-related ignitions concurrent with high winds promote large wildfires across the USA. *International Journal of Wildland Fire*, *27*(6), 377–386. https://doi.org/10.1071/WF17149

Abatzoglou, J. T., & Williams, A. P. (2016). Impact of anthropogenic climate change on wildfire across western US forests. *Proceedings of the National Academy of Sciences of the United States of America*, *113*(42), 11770–11775. https://doi.org/10.1073/pnas.1607171113

Abatzoglou, J. T., Williams, A. P., Boschetti, L., Zubkova, M., & Kolden, C. A. (2018). Global patterns of interannual climate-fire relationships. *Global Change Biology*, *24*(11), 5164–5175. https://doi.org/10.1111/gcb.14405

Abolafia-Rosenzweig, R., He, C., & Chen, F. (2022). Winter and spring climate explains a large portion of interannual variability and trend in western U.S. summer fire burned area. *Environmental Research Letters*, *17*(5), 054030. https://doi.org/10.1088/1748-9326/ac6886

Almazroui, M., Islam, M. N., Saeed, F., Saeed, S., Ismail, M., Ehsan, M. A., et al. (2021). Projected changes in temperature and precipitation over the United States, Central America, and the Caribbean in CMIP6 GCMs. *Earth Systems and Environment*, *5*, 1–24. https://doi.org/10.1007/s41748-021-00199-5

Baijnath-Rodino, J. A., Martinez, A., York, R. A., Foufoula-Georgiou, E., AghaKouchak, A., & Banerjee, T. (2023). Quantifying the effectiveness of shaded fuel breaks from ground-based, aerial, and spaceborne observations. *Forest Ecology and Management*, *543*, 121142. https://doi.org/10.1016/j.foreco.2023.121142

Balch, J. K., Bradley, B. A., Abatzoglou, J. T., Nagy, R. C., Fusco, E. J., & Mahood, A. L. (2017). Human-started wildfires expand the fire niche across the United States. *Proceedings of the National Academy of Sciences of the United States of America*, *114*(11), 2946–2951. https://doi.org/10.1073/pnas.1617394114

Boisramé, G. F. S., Brown, T. J., & Bachelet, D. M. (2022). Trends in western USA fire fuels using historical data and modeling. *Fire Ecology*, *18*(1), 8. https://doi.org/10.1186/s42408-022-00129-4

Borgonovo, E. (2007). A new uncertainty importance measure. *Reliability Engineering & System Safety*, *92*(6), 771–784. https://doi.org/10.1016/j.ress.2006.04.015

Bradshaw, L. S., Deeming, J. E., Burgan, R. E., & Cohen, J. D. (1984). *The 1978 national fire-danger rating system: Technical documentation* (No. INT-GTR-169). U.S. Department of Agriculture, Forest Service, Intermountain Forest and Range Experiment Station. https://doi.org/10.2737/INT-GTR-169

Brotons, L., Aquilué, N., de Cáceres, M., Fortin, M.-J., & Fall, A. (2013). How fire history, fire suppression practices and climate change affect wildfire regimes in Mediterranean landscapes. *PLoS One*, *8*(5), e62392. https://doi.org/10.1371/journal.pone.0062392

Brown, E. K., Wang, J., & Feng, Y. (2021). US wildfire potential: A historical view and future projection using high-resolution climate data. *Environmental Research Letters*, *16*(3), 034060. https://doi.org/10.1088/1748-9326/aba868

Burgan, R., Hardy, C., Ohlen, D., Fosnight, G., & Treder, R. (1999). *Ground sample data for the conterminous U.S. Land cover characteristics Database* (No. RMRS-GTR-41). U.S. Department of Agriculture, Forest Service, Rocky Mountain Research Station. https://doi.org/10.2737/RMRS-GTR-41

Burgan, R., Klaver, R., & Klaver, J. (1998). Fuel models and fire potential from satellite and surface observations. *International Journal of Wildland Fire*, *8*(3), 159. https://doi.org/10.1071/WF9980159

Burgan, R. E., Hardy, C. C., & Fosnight, G. (1997). *Landcover ground sample data (general technical report)*. INT-GTR-368CD. United States Department of Agriculture, Forest Service.

Byram, G. M. (1959). Combustion of forest fuels. In *Forest fire: Control and use* (pp. 61–89).

CEC. (1999). *A proposed framework for delineating ecologically-based planning, implementation, and evaluation units for cooperative bird conservation in the U.S.; Ecological regions of North America: Toward a common perspective*. Commission for Environmental Cooperation.

Cruz, M. G., & Plucinski, M. P. (2007). *Billo road fire: Report on fire behaviour phenomena and suppression activities*. Bushfire Cooperative Research Centre.

Daly, C., Halbleib, M., Smith, J. I., Gibson, W. P., Doggett, M. K., Taylor, G. H., et al. (2008). Physiographically sensitive mapping of climatological temperature and precipitation across the conterminous United States. *International Journal of Climatology: A Journal of Royal Meteorological Society*, *28*(15), 2031–2064. https://doi.org/10.1002/joc.1688

Deeming, J. E., Burgan, R. E., & Cohen, J. D. (1977). *The national fire danger rating system* (No. INT-GTR-39). U.S. Department of Agriculture, Forest Service, Intermountain Forest and Range Experiment Station.

Dennison, P. E., Brewer, S. C., Arnold, J. D., & Moritz, M. A. (2014). Large wildfire trends in the western United States, 1984–2011. *Geophysical Research Letters*, *41*(8), 2928–2933. https://doi.org/10.1002/2014GL059576

Di Giuseppe, F., Pappenberger, F., Wetterhall, F., Krzeminski, B., Camia, A., Libertá, G., & San Miguel, J. (2016). The potential predictability of fire danger provided by numerical weather prediction. *Journal of Applied Meteorology and Climatology*, *55*(11), 2469–2491. https://doi.org/10.1175/JAMC-D-15-0297.1

Donner, L. J., Wyman, B. L., Hemler, R. S., Horowitz, L. W., Ming, Y., Zhao, M., et al. (2011). The dynamical core, physical parameterizations, and basic simulation characteristics of the atmospheric component AM3 of the GFDL global coupled model CM3. *Journal of Climate*, *24*(13), 3484–3519. https://doi.org/10.1175/2011JCLI3955.1

Easterling, D. R., Arnold, J. R., Knutson, T., Kunkel, K. E., LeGrande, A. N., Leung, L. R., et al. (2017). Ch. 7: Precipitation change in the United States. In *Climate science special report: Fourth national climate assessment* (Vol. I). U.S. Global Change Research Program. https://doi.org/10.7930/J0H993CC

Eidenshink, J., Schwind, B., Brewer, K., Zhu, Z.-L., Quayle, B., & Howard, S. (2007). A project for monitoring trends in Burn severity [Dataset]. Fire Ecology, *3*(1), 3–21. https://doi.org/10.4996/fireecology.0301003

Eidenshink, J. C., & Howard, S. M. (2012). *United States Geological Survey fire science: Fire danger monitoring and forecasting (USGS numbered series no. 2012–3121), United States Geological Survey fire science: Fire danger monitoring and forecasting*. Fact Sheet. U.S. Geological Survey. https://doi.org/10.3133/fs20123121

Ficklin, D. L., Maxwell, J. T., Letsinger, S. L., & Gholizadeh, H. (2015). A climatic deconstruction of recent drought trends in the United States. *Environmental Research Letters*, *10*(4), 044009. https://doi.org/10.1088/1748-9326/10/4/044009

Finney, M. A. (2006). An overview of FlamMap fire modeling capabilities. In *Andrews Patricia Butl. Bret W Comps 2006 fuels Manag.- Meas. Success Conf. Proc. 28–30 March 2006 Portland Proc. RMRS-P-41 Fort Collins CO US Dep. Agric. For. Serv. Rocky Mt. Research Station. P 213-220 041*.

Finney, M. A., McHugh, C. W., Grenfell, I. C., Riley, K. L., & Short, K. C. (2011). A simulation of probabilistic wildfire risk components for the continental United States. *Stochastic Environmental Research and Risk Assessment*, *25*(7), 973–1000. https://doi.org/10.1007/s00477-011-0462-z

Flanagan, B. E., Hallisey, E. J., Adams, E., & Lavery, A. (2018). Measuring community vulnerability to natural and anthropogenic hazards: The centers for disease control and prevention's social vulnerability index. *Journal of Environmental Health*, *80*, 3.

Fosberg, M. A., & Deeming, J. E. (1971). *Derivation of the 1- and 10-hour timelag fuel moisture calculations for fire-danger rating* (No. Research Note RM-RN-207). USDA Forest Service, Rocky Mountain Forest and Range Experiment Station.

Freeborn, P. H., Jolly, W. M., & Cochrane, M. A. (2016). Impacts of changing fire weather conditions on reconstructed trends in U.S. wildland fire activity from 1979 to 2014: Reconstructed Trends in U.S. Fire Activity. *Journal of Geophysical Research: Biogeosciences*, *121*(11), 2856–2876. https://doi.org/10.1002/2016JG003617

Gamelin, B. L., Feinstein, J., Wang, J., Bessac, J., Yan, E., & Kotamarthi, V. R. (2022). Projected U.S. drought extremes through the twenty first century with vapor pressure deficit. *Scientific Reports*, *12*(1), 8615. https://doi.org/10.1038/s41598-022-12516-7

Gent, P. R., Danabasoglu, G., Donner, L. J., Holland, M. M., Hunke, E. C., Jayne, S. R., et al. (2011). The community climate system model version 4. *Journal of Climate*, *24*(19), 4973–4991. https://doi.org/10.1175/2011JCLI4083.1

Gleason, K. E., McConnell, J. R., Arienzo, M. M., Chellman, N., & Calvin, W. M. (2019). Four-fold increase in solar forcing on snow in western U.S. burned forests since 1999. *Nature Communications*, *10*(1), 2026. https://doi.org/10.1038/s41467-019-09935-y

Goward, S. N., Markham, B., Dye, D. G., Dulaney, W., & Yang, J. (1991). Normalized difference vegetation index measurements from the advanced very high resolution radiometer. *Remote Sensing of Environment*, *35*(2–3), 257–277. https://doi.org/10.1016/0034-4257(91)90017-Z

Gutzler, D. S., & Robbins, T. O. (2011). Climate variability and projected change in the western United States: Regional downscaling and drought statistics. *Climate Dynamics*, *37*(5–6), 835–849. https://doi.org/10.1007/s00382-010-0838-7

Hardy, C. C., & Hardy, C. E. (2007). Fire danger rating in the United States of America: An evolution since 1916. *International Journal of Wildland Fire*, *16*(2), 217. https://doi.org/10.1071/WF06076

Herman, J., & Usher, W. (2017). SALib: An open-source Python library for Sensitivity Analysis. *Journal of Open Source Software*, *2*(9), 97. https://doi.org/10.21105/joss.00097

Iglesias, V., Balch, J. K., & Travis, W. R. (2022). U.S. fires became larger, more frequent, and more widespread in the 2000s. *Science Advances*, *8*(11), eabc0020. https://doi.org/10.1126/sciadv.abc0020

Jay, A., Reidmiller, D. R., Avery, C. W., Barrie, D., DeAngelo, B. J., Dave, A., et al. (2018). Chapter 1: Overview. In *Impacts, risks, and adaptation in the United States: The fourth national climate assessment* (Vol. II). U.S. Global Change Research Program. https://doi.org/10.7930/NCA4.2018.CH1

Jolly, W. M. (2018). Overview of NFDRS 2016.

Jones, C. D., Hughes, J. K., Bellouin, N., Hardiman, S. C., Jones, G. S., Knight, J., et al. (2011). The HadGEM2-ES implementation of CMIP5 centennial simulations. *Geoscientific Model Development*, *4*(3), 543–570. https://doi.org/10.5194/gmd-4-543-2011

Keetch, J. J., & Byram, G. M. (1968). A drought index for forest fire control SE-38 U.S.D.A. For. Serv. Res. Pap.

Klaver, J., Klaver, R., & Burgan, R. E. (1997). Using GIS to assess forest fire hazard in the Mediterranean region of the United States. In *17th annual ESRI users Conference*. San Diego, CA.

López, A. S., San-Miguel-Ayanz, J., & Burgan, R. E. (2002). Integration of satellite sensor data, fuel type maps and meteorological observations for evaluation of forest fire risk at the pan-European scale. *International Journal of Remote Sensing*, *23*(13), 2713–2719. https://doi.org/10.1080/01431160110107761

Loveland, T., Merchant, J., Brown, J., & Ohlen, D. (1991). Development of a land-cover characteristics database for the conterminous. *U. S. Photogrammetric Engineering and Remote Sensing*, *57*, 1453–1463.

Lynch, C., Seth, A., & Thibeault, J. (2016). Recent and projected annual cycles of temperature and precipitation in the northeast United States from CMIP5. *Journal of Climate*, *29*(1), 347–365. https://doi.org/10.1175/JCLI-D-14-00781.1

Mann, H. B. (1945). Nonparametric tests against trend. *Econometrica*, *13*(3), 245–259. https://doi.org/10.2307/1907187

Mitchell, K. E., Lohmann, D., Houser, P. R., Wood, E. F., Schaake, J. C., Robock, A., et al. (2004). The multi-institution North American Land Data Assimilation System (NLDAS): Utilizing multiple GCIP products and partners in a continental distributed hydrological modeling system. *Journal of Geophysical Research*, *109*(D7). https://doi.org/10.1029/2003JD003823

NCAR. (2023). The codes were downloaded from the NCAR github repository. Retrieved from https://github.com/NCAR/fire-indices

NIFC. (2020). *Historical wildland fire information and federal firefighting costs*. National Interagency Fire Center.

Plischke, E., Borgonovo, E., & Smith, C. L. (2013). Global sensitivity measures from given data. *European Journal of Operational Research*, *226*(3), 536–550. https://doi.org/10.1016/j.ejor.2012.11.047

Preisler, H. K., Burgan, R. E., Eidenshink, J. C., Klaver, J. M., & Klaver, R. W. (2009). Forecasting distributions of large federal-lands fires utilizing satellite and gridded weather information. *International Journal of Wildland Fire*, *18*(5), 508–516. https://doi.org/10.1071/WF08032

Preisler, H. K., Eidenshink, J., Howard, S., & Burgan, R. E. (2015). Forecasting distribution of numbers of large fires. In *Keane Robert E Jolly Matt Parsons Russell Riley Karin Proc. Large wildland fires Conf. May 19-23 2014 Missoula MT Proc RMRS-P-73 Fort Collins CO US Dep. Agric. For. Serv. Rocky Mt. Res. Stn* (pp. 181–187).

Skamarock, C., Klemp, B., Dudhia, J., Gill, O., Barker, D., Duda, G., et al. (2008). A description of the advanced research WRF version 3. https://doi.org/10.5065/D68S4MVH

Sobol, I. M. (2001). Global sensitivity indices for nonlinear mathematical models and their Monte Carlo estimates. *Mathematics and Computers in Simulation*, *55*(1–3), 271–280. https://doi.org/10.1016/S0378-4754(00)00270-6

Spearman, C. (1904). The proof and measurement of association between two things. *American Journal of Psychology*, *15*(1), 72–101. https://doi.org/10.2307/1412159

Steel, Z. L., Safford, H. D., & Viers, J. H. (2015). The fire frequency-severity relationship and the legacy of fire suppression in California forests. *Ecosphere*, *6*(1), 1–23. art8. https://doi.org/10.1890/ES14-00224.1

Sturtevant, B. R., & Cleland, D. T. (2007). Human and biophysical factors influencing modern fire disturbance in northern Wisconsin. *International Journal of Wildland Fire*, *16*(4), 398–413. https://doi.org/10.1071/WF06023

Sudiana, D., Kuze, H., Takeuchi, N., & Burgan, R. E. (2003). Assessing forest fire potential in Kalimantan Island, Indonesia, using satellite and surface weather data. *International Journal of Wildland Fire*, *12*(2), 175. https://doi.org/10.1071/WF02035

Taylor, K. E., Stouffer, R. J., & Meehl, G. A. (2012). An overview of CMIP5 and the experiment design. *Bulletin of the American Meteorological Society*, *93*(4), 485–498. https://doi.org/10.1175/BAMS-D-11-00094.1

Taylor, S. W., & Alexander, M. E. (2006). Science, technology, and human factors in fire danger rating: The Canadian experience. *International Journal of Wildland Fire*, *15*(1), 121. https://doi.org/10.1071/WF05021

Tian, X., Shu, L., Zhao, F., Wang, M., & McRae, D. J. (2011). Future impacts of climate change on forest fire danger in northeastern China. *Journal of Forestry Research*, *22*(3), 437–446. https://doi.org/10.1007/s11676-011-0185-5

Vermote, E. (2019). NOAA climate data Record (CDR) of AVHRR normalized difference vegetation Index (NDVI), version 5 [Dataset]. https://doi.org/10.7289/V5ZG6QH9

Wagner, C. E. V. (1974). *STRUCTURE OF THE CANADIAN FOREST FIRE WEATHER INDEX (No. Fo47-1333)*. DEPARTMENT OF THE ENVIRONMENT, Canadian Forestry Service.

Wagner, C. E. V. (1987). *Development and structure of the Canadian forest fire weather Index system, forestry technical report*. Canada Communication Group Publ.

Wang, J., & Kotamarthi, V. R. (2015). High-resolution dynamically downscaled projections of precipitation in the mid and late 21st century over North America. *Earth's Future*, *3*(7), 268–288. https://doi.org/10.1002/2015EF000304

Westerling, A. L. (2016). Increasing western US forest wildfire activity: Sensitivity to changes in the timing of spring. *Philosophical Transactions of the Royal Society B: Biological Sciences*, *371*(1696), 20150178. https://doi.org/10.1098/rstb.2015.0178

Wu, Q., Bessac, J., Huang, W., & Wang, J. (2022). Station-wise statistical joint assessment of wind speed and direction under future climates across the United States. https://doi.org/10.48550/arXiv.2205.02936